Journal of Solid State Chemistry **160,** 230–238 (2001)
doi:10.1006/jssc.2001.9227, available online at http://www.idealibrary.com on IDEAL®

Negative Thermal Expansion in Orthorhombic $NbOPO_4$

T. G. Amos[1] and A. W. Sleight[2]

Department of Chemistry, Oregon State University, Corvallis, Oregon 97330-4003

Received January 23, 2001; in revised form April 18, 2001; accepted April 30, 2001

Monoclinic $NbOPO_4$ was found to undergo a readily reversible first-order phase transition at 292°C. The connectivity of the NbO_6 octahedra and PO_4 tetrahedra remains the same throughout the transition, but above the transition the symmetry has increased to orthorhombic and Z has decreased by a factor of 2. Rietveld structure refinements utilized neutron diffraction data from room temperature to 400°C and X-ray diffraction data up to 700°C. One cell edge shows negative thermal expansion over the entire temperature range. The other two cell edges show negative thermal expansion only above the phase transition. The negative thermal expansion behavior is related to transverse thermal motion of oxygen. © 2001 Academic Press

INTRODUCTION

Two different structures are known for $NbOPO_4$ (Fig. 1). Both are based on NbO_6 octahedra and PO_4 tetrahedra, which share corners to form three-dimensional networks. In both structures, the NbO_6 octahedra link to each other to form chains. In tetragonal $NbOPO_4$, two opposite corners of the NbO_6 octahedra are used to form linear chains along the *c* axis (1). In monoclinic $NbOPO_4$, two adjacent corners of the NbO_6 octahedra are used to form zigzag chains along the *b* axis (2). An orthorhombic version of this same structure at room temperature has also been reported from single-crystal X-ray diffraction data (3).

We have been systematically investigating the thermal expansion properties of $AOMO_4$ compounds based on AO_6 octahedra and MO_4 tetrahedra. Because all oxygen atoms are in two-fold coordination, negative thermal expansion behavior might occur based on the transverse thermal motion of oxygen. In our study of tetragonal $NbOPO_4$, we discovered a phase transition at about 200°C (4). All cell edges showed positive thermal expansion below the transition, but negative thermal expansion was observed for the *a* and *b* axes above the transition. The thermal expansion properties of monoclinic and orthorhombic $NbOPO_4$ have not been reported.

EXPERIMENTAL

A five-fold excess of phosphoric acid (85%) was placed with Nb_2O_5 (Alfa Aesar, 99.9 + %) in a Pt crucible. The slurry was stirred and then heated to 1300°C at a rate of 300°C/hour. The sample was maintained at this temperature for 90 minutes and then air-quenched from the reaction temperature. If this sample is not quenched, a mixture of the tetragonal and monoclinic $NbOPO_4$ polymorphs results.

Differential scanning calorimetry (DSC) measurements were obtained on a TA Instruments differential scanning calorimeter 2920 over the temperature range of 20 to 550°C. The sample was heated at a rate of 10°C/minute in an aluminum pan under a flow of N_2.

Neutron powder diffraction data were collected on the BT-1 diffractometer at the Center for Neutron Research at the National Institute of Standards and Technology, using a Cu(311) monochromator with a λ of 1.5402(2) Å, and an array of 32 He-3 detectors at 5° intervals. The sample was sealed in a vanadium sample container of length 50 mm and a diameter of 15.6 mm inside a dry He-filled glovebox. Diffraction measurements were collected at four different temperatures: 25, 200, 325, and 400°C in a closed-cycle He gas high-temperature unit.

X-ray powder diffraction data were collected over the temperature range 20 to 700°C on an INEL diffractometer with monochromatic Cu$K\alpha$ radiation and a position-sensitive detector. A small amount of ethanol was mixed with the sample and Si (NIST SRM 640b internal standard). This slurry was dropped onto the sample holder and the solvent was allowed to evaporate. This rotating holder was placed in a resistively heated furnace attachment to collect diffraction data above room temperature. All refinements were performed using GSAS software (5).

[1]Current address: National Institute of Standards and Technology, NIST Center for Neutron Research, 100 Bureau Dr., Stop 8562, Gaithersburg, MD 20899-8562

[2]To whom correspondence should be addressed. Fax: 541-737-2062. E-mail: arthur.sleight@orst.edu.

0022-4596/01 $35.00

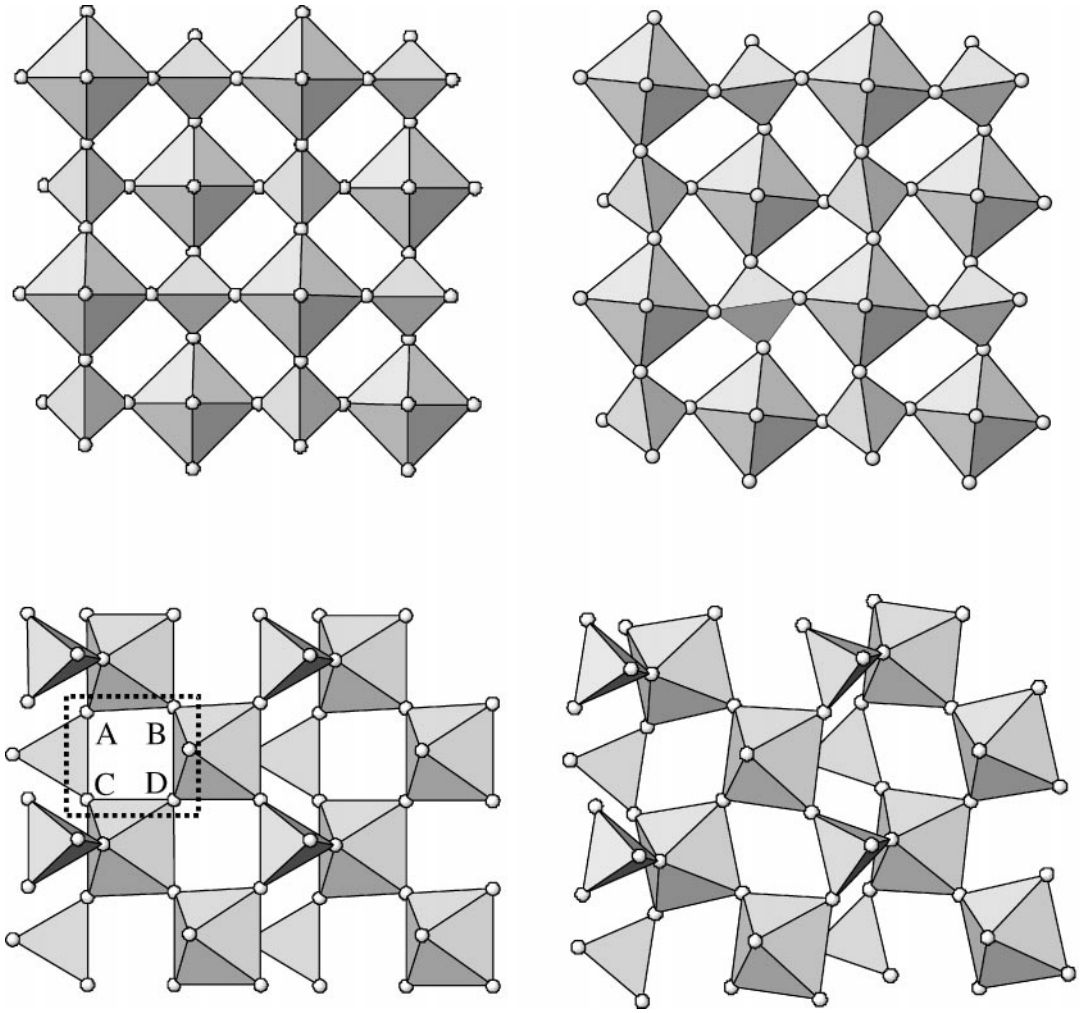

FIG. 1. Structures of $NbOPO_4$. Upper left, the high-temperature tetragonal form. Upper right, the low-temperature tetragonal form. Lower left and right, the orthorhombic and monoclinic forms, respectively.

RESULTS

Our DSC data (Fig. 2) for monoclinic $NbOPO_4$ show an endothermic peak on heating and an exothermic peak on cooling. There is, therefore, a readily reversible, first-order transition with an onset temperature on both heating and cooling of about 292°C.

A Rietveld refinement of our room-temperature neutron diffraction data for monoclinic $NbOPO_4$ was initiated in space group $P2_1/c$ with the positional parameters reported from single-crystal X-ray diffraction data (2). Our refined positional parameters (Table 1) are in good agreement with those published.

Examination of our diffraction patterns above the 292°C phase transition indicated that the patterns had become simpler. In fact, the patterns above 292°C could be accounted for on the basis of the 11.3- $\times$ 5.3- $\times$ 6.6-Å orthorhombic cell (space group *Pnma*) given by Serra and Hwu (3). Because the monoclinic and orthorhombic versions of $NbOPO_4$ are basically the same, we converted the $a = 13.097$ Å, $b = 5.280$ Å, $c = 13.228$ Å, $\beta = 120.334°$ monoclinic cell given by LeClaire *et al.* (2) into a cell with $a = 11.304$ Å, $b = 5.280$ Å, $c = 13.228$ Å, $\beta = 90.002°$. The c axis in the monoclinic cell is twice that in the orthorhombic cell. If β were really this close to 90° at room temperature, powder diffraction data would appear to arise from an orthorhombic cell. In fact, we find a β angle of 90.34° at room temperature. This is a sufficient deviation from 90° to show split peaks at room temperature.

Rietveld refinements were conducted on all neutron and X-ray diffraction data collected at the various temperatures. The refinements based on neutron data yield more accurate positional and thermal displacement parameters for the light atoms. Therefore, only these results are presented in

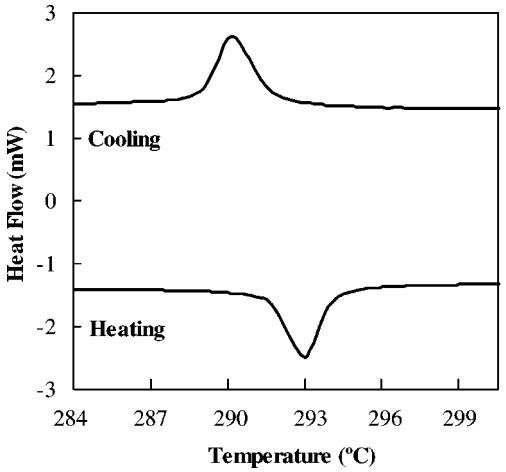

FIG. 2. Differential scanning calorimetry starting at room temperature with monoclinic $NbOPO_4$.

detail over the temperature range where both XRD and neutron data were obtained. The cell dimensions from the X-ray diffraction data should be as accurate as those obtained from the neutron diffraction data.

TABLE 1
Atomic Coordinates for Monoclinic $NbOPO_4$ at 25 and 200°C

Atom	*x/a*	*y/b*	*z/c*
Nb(1)	0.0628(4)[a]	0.244(1)	0.3658(3)
	0.0629(4)	**0.244(1)**	**0.3662(4)**
Nb(2)	0.5641(3)	0.246(1)	0.1985(3)
	0.5640(4)	**0.248(1)**	**0.1985(4)**
P(1)	0.3452(4)	0.257(1)	0.4079(4)
	0.3448(5)	**0.259(1)**	**0.4093(5)**
P(2)	0.1552(4)	0.770(1)	0.0637(4)
	0.1538(5)	**0.765(1)**	**0.0632(5)**
O(1)	0.2154(4)	0.242(1)	0.3708(4)
	0.2148(5)	**0.239(1)**	**0.3708(5)**
O(2)	0.9175(4)	0.234(1)	0.3752(4)
	0.9180(5)	**0.239(1)**	**0.3757(5)**
O(3)	0.0089(5)	0.5403(9)	0.2689(5)
	0.0077(6)	**0.533(1)**	**0.2651(5)**
O(4)	0.1403(5)	0.473(1)	0.5115(5)
	0.1385(5)	**0.476(1)**	**0.5099(6)**
O(5)	0.1169(5)	−0.060(1)	0.4698(5)
	0.1181(5)	**−0.057(1)**	**0.4708(5)**
O(6)	0.7139(4)	0.232(1)	0.3434(4)
	0.7147(5)	**0.239(1)**	**0.3430(5)**
O(7)	0.4189(4)	0.286(1)	0.0403(4)
	0.4178(5)	**0.285(1)**	**0.0400(5)**
O(8)	0.4978(5)	0.471(1)	0.2634(4)
	0.4964(6)	**0.471(1)**	**0.2615(5)**
O(9)	0.6279(5)	0.024(1)	0.1199(5)
	0.6284(6)	**0.020(1)**	**0.1218(5)**
O(10)	0.6279(5)	0.555(1)	0.1569(5)
	0.6283(5)	**0.550(1)**	**0.1548(5)**

[a]Bold values are for 200°C; others are for 25°C.

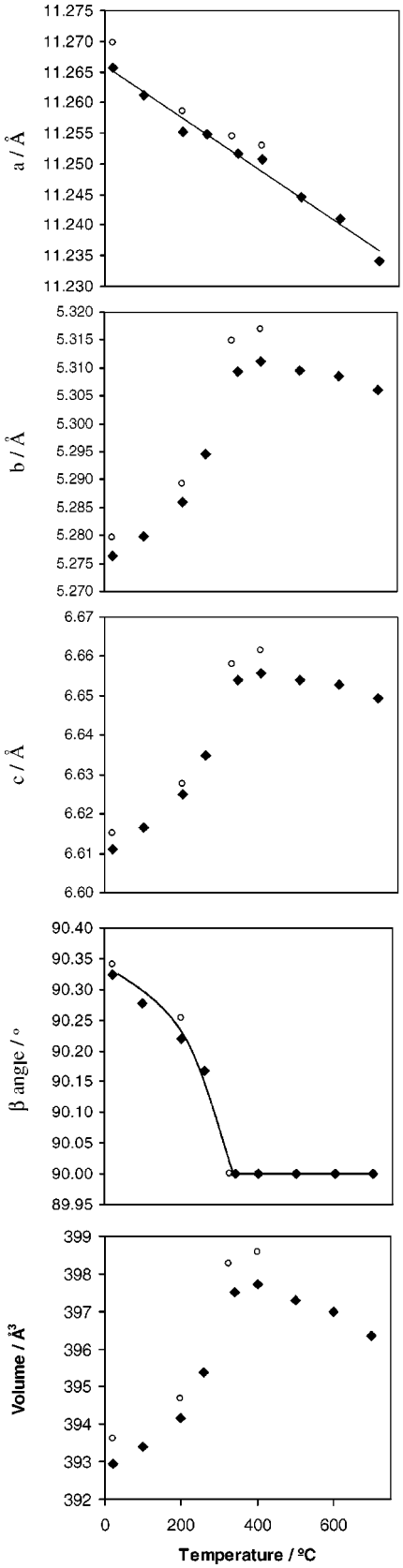

FIG. 3. Cell edges, β angle, and cell volume vs temperature.

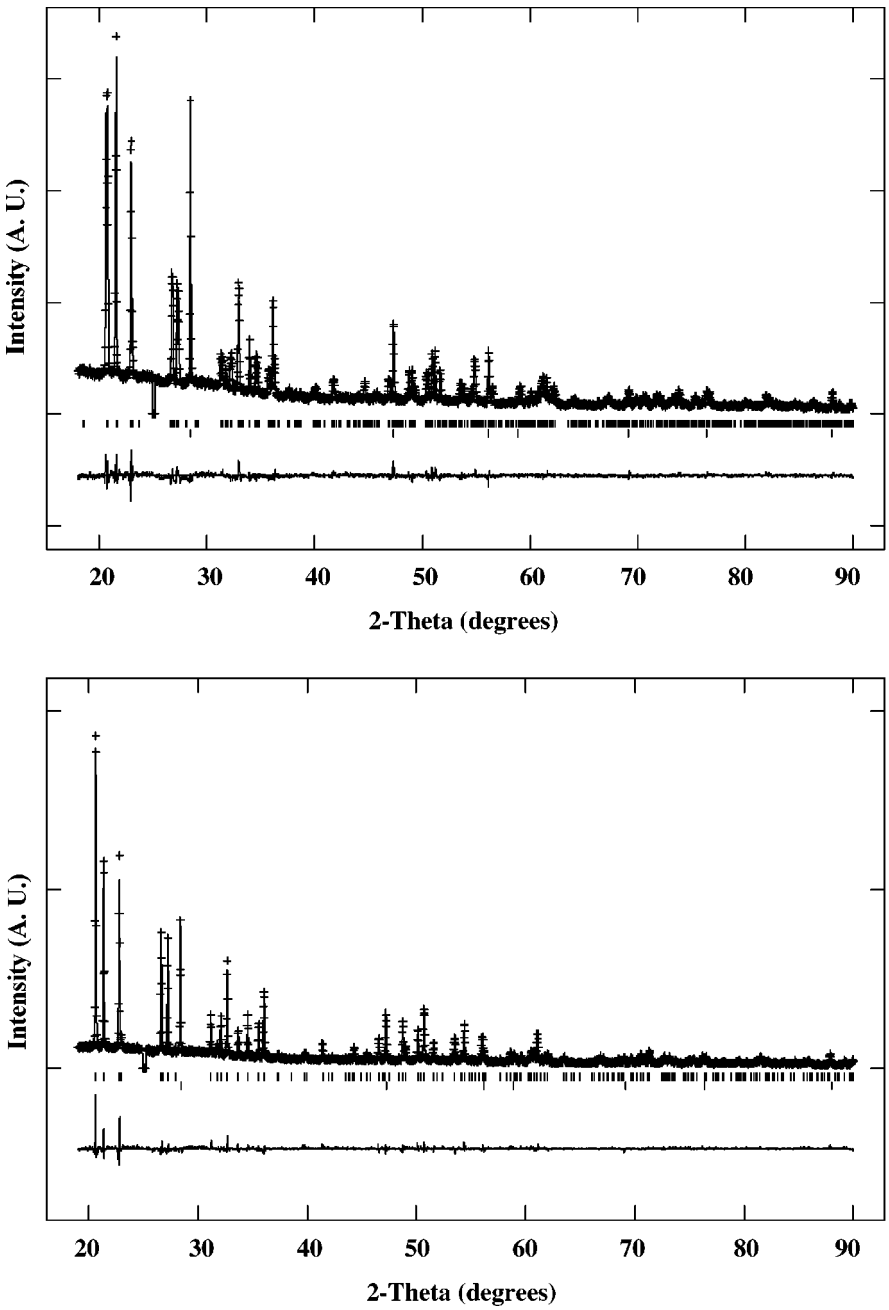

FIG. 4. Rietveld fits of neutron data taken at 25°C (upper) and 340°C (lower). Second phase is Si internal standard. Excluded regions are due to an instrumental artifact.

The cell dimensions for monoclinic and orthorhombic $NbOPO_4$ are shown as a function of temperature in Fig. 3. Although refinements were conducted in the standard monoclinic cell with $\beta \sim 120^\circ$, the cell edges and β were converted to the pseudo-orthorhombic cell with c divided by 2 for the purposes of these plots. Negative thermal expansion is exhibited by the a cell edge over the entire range of measurement. No change in the thermal expansion coefficient for the a cell edge can be detected at the phase transition. The b and c cell edges show strong positive thermal expansion below the transition. The first two points for these edges above the transition, points at 325 and 400°C, indicate weak positive thermal expansion from both X-ray and neutron data. Above 400°C, both the b and c cell edges show negative thermal expansion. The actual values for the thermal expansion coefficients are given in Table 2 for the various temper-

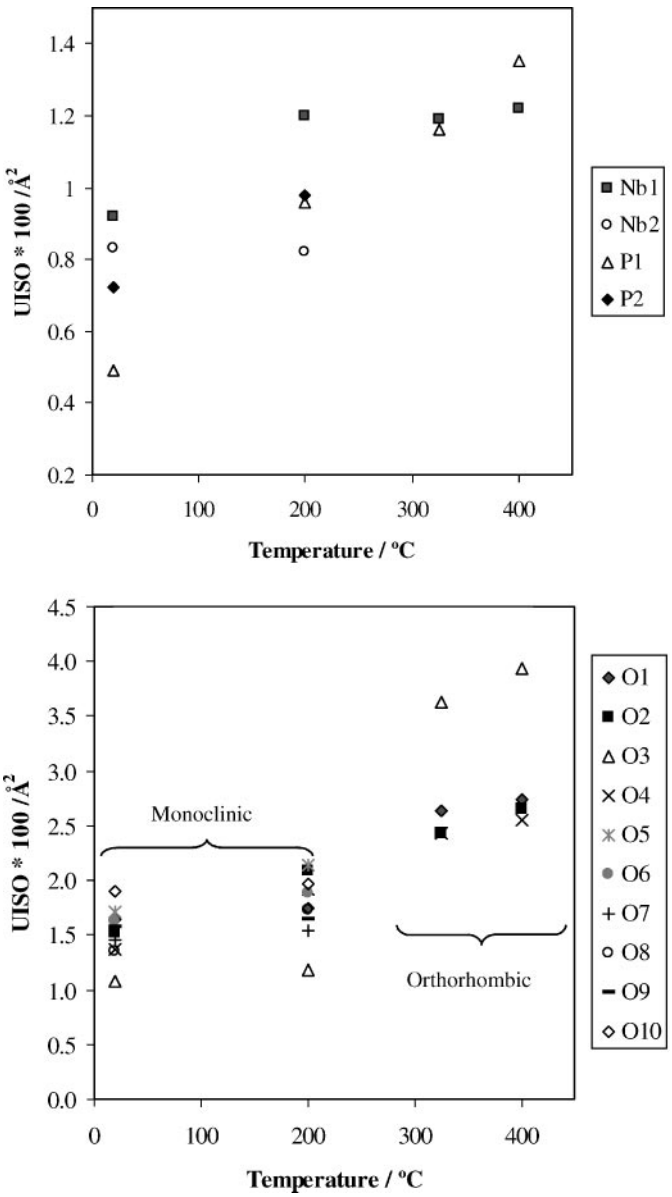

FIG. 5. Isotropic displacement factors vs temperature.

ature ranges. The β angle decreases steadily from 90.35° at room temperature to 90.16° at 250°C before dropping to 90.0° by 325°C, presumably dropping to 90.0° at 292°C.

Refined positional parameters from the neutron data obtained at the various temperatures are given in Tables 1 and 3. Representative Rietveld fits are given in Fig. 4, and statistics for these Rietveld refinements are given in Table 4. Interatomic distances are given in Tables 5 and 6. Note that the average Nb–O distance remains constant at 1.955(5) Å over the entire temperature range. A plot of isotropic thermal displacements vs temperature is given in Fig. 5. A portion of the orthorhombic $NbOPO_4$ structure is shown in Fig. 6 with thermal ellipsoids. The magnitudes of the

TABLE 2
Thermal Expansion Coefficients[a] for $NbOPO_4$

Temperature range (°C)	Cell dimension	α ($°C^{-1}$)
20–340	a	-3.86×10^{-6}
	b	1.89×10^{-5}
	c	1.95×10^{-5}
	Volume	3.46×10^{-5}
	α_l	1.15×10^{-5}
400–700	a	-4.76×10^{-6}
	b	-3.11×10^{-6}
	c	-3.13×10^{-6}
	Volume	-1.10×10^{-5}
	α_l	-3.67×10^{-6}

[a] α_l = average linear expansion.

U values along the principal axes of the ellipsoids are given in Table 7.

DISCUSSION

We can expect that negative thermal expansion will result either from a decrease in M–O–M angles with increasing temperature or from a decrease in apparent M–O distances with increasing temperature. The strongest negative thermal expansion behavior for orthorhombic $NbOPO_4$ is observed

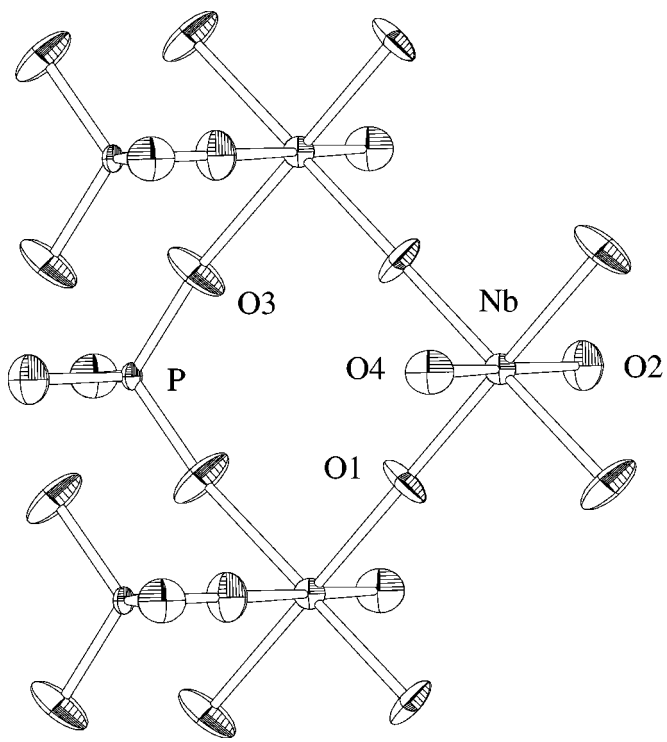

FIG. 6. Portion of the $NbOPO_4$ structure at 400°C showing thermal ellipsoids.

TABLE 3
Atomic Coordinates for Orthorhombic $NbOPO_4$ at 325 and 400°C

Atom	*x/a*	*y/b*	*z/c*
Nb	0.4384(3)[a]	$\frac{1}{4}$	0.3291(5)
	0.4377(2)		**0.3302(4)**
P	0.1539(4)	$\frac{1}{4}$	0.5285(6)
	0.1534(3)		**0.5288(5)**
O(1)	0	0	0
O(2)	0.0807(7)	$\frac{1}{4}$	0.3333(7)
	0.0807(3)		**0.3350(5)**
O(3)	0.1285(3)	0.0166(7)	0.6448(5)
	0.1278(2)	**0.0162(5)**	**0.6462(4)**
O(4)	0.2852(4)	$\frac{1}{4}$	0.4714(7)
	0.2850(3)		**0.4709(5)**

[a]Bold values are for 400°C; others are for 325°C.

TABLE 4
Neutron Diffraction Refinement Statistics[a] for $NbOPO_4$

Temp (°C)	χ^2	wR_p	R_p
25	2.019	0.0716	0.0561
200	1.858	0.0685	0.0543
325	2.202	0.0942	0.0749
400	1.686	0.0658	0.0528

[a]$\chi^2 = \sum w(I_{obs} - I_{calc})^2/(N_{obs} - N_{var})$; $R_p = \sum|I_{obs} - I_{calc}|/\sum I_{obs}$; $wR_p = [\sum w(I_{obs} - I_{calc})^2/\sum wI_{obs}{}^2]^{1/2}$.

from 400 to 700°C. Over that range, there is no indication that Nb–O–Nb or Nb–O–P angles are decreasing (Fig. 7). Likewise, Nb–O distances are not decreasing. There is, however, a significant decrease in the P–O bond distance from 1.535 to 1.495 Å over this temperature range (Fig. 8). Given the standard deviations of 0.01 Å on individual P–O bonds, this decrease in P–O bond distance with increasing temperature cannot be considered in a quantitative manner. However, qualitatively this decrease supports a model whereby the thermal contraction of the unit cell above 400°C is due to the thermal motion of oxygen in the Nb–O–P linkages. The Nb–O distances of this linkage show no indication of decreasing on heating from 400 to 700°C, although these distances should be influenced the same as the P–O distances by the transverse thermal motion of oxygen in the Nb–O–P linkages. A similar situation has been observed for $Y_2W_3O_{12}$ where the apparent W–O distance decreases with increasing temperature, but the Y–O distance does not (6). Presumably, there is some real thermal expansion of the Nb–O and Y–O bond lengths, which compensates for the contraction effect expected for the transverse thermal motion of oxygen. Thus, the apparent bond distance shortening is apparent only in the stronger (W–O or P–O) distances, which are not expected to change any significant real extent with temperature.

The situations for tetragonal $NbOPO_4$ and monoclinic $NbOPO_4$ are very similar in some respects. Both have

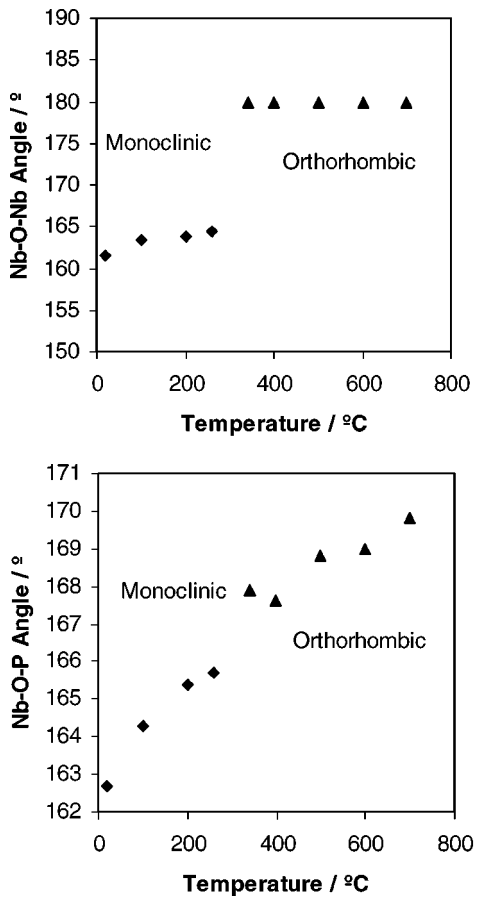

FIG. 7. Average Nb–O–Nb and Nb–O–P angles vs temperature.

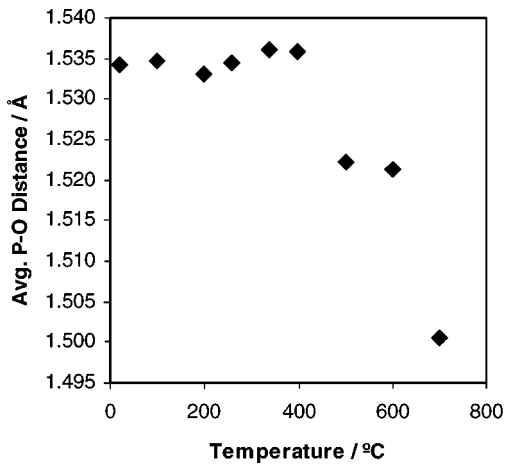

FIG. 8. Average P–O distance vs temperature.

TABLE 5
Selected Bond Distances for 25 and 200°C Data

Nb(1)–O(1)	Nb(1)–O(2)	Nb(1)–O(3)	Nb(1)–O(3)	Nb(1)–O(4)	Nb(1)–O(5)
1.967(6)[a]	1.971(6)	1.914(7)	1.873(7)	2.049(7)	1.997(8)
1.959(7)	**1.966(7)**	**1.914(8)**	**1.868(8)**	**2.045(9)**	**1.992(10)**
Nb(2)–O(6)	Nb(2)–O(7)	Nb(2)–O(8)	Nb(2)–O(8)	Nb(2)–O(9)	Nb(2)–O(10)
1.923(6)	1.995(6)	1.915(8)	1.854(8)	2.008(7)	2.034(8)
1.926(7)	**2.004(7)**	**1.904(8)**	**1.867(8)**	**2.018(9)**	**2.023(10)**
P(1)–O(1)	P(1)–O(7)	P(1)–O(9)	P(1)–O(10)		
1.512(6)	1.525(7)	1.543(8)	1.519(8)		
1.540(8)	**1.541(8)**	**1.531(9)**	**1.527(8)**		
P(2)–O(2)	P(2)–O(4)	P(2)–O(5)	P(2)–O(6)		
1.543(6)	1.492(8)	1.544(8)	1.530(6)		
1.543(8)	**1.539(9)**	**1.546(8)**	**1.513(8)**		

[a]Bold values are for 200°C; others are for 25°C.

displacive phase transitions not far above room temperature. Tetragonal $NbOPO_4$ shows negative thermal expansion behavior only above the phase transition (4). The negative thermal expansion behavior for monoclinic $NbOPO_4$ becomes much more pronounced above the phase transition, where the lattice symmetry is orthorhombic. In both cases the rocking motions of the polyhedra that contribute to negative thermal expansion at high temperature freeze out on cooling through the phase transition, giving a structure with lower symmetry. However, the displacive phase transition between monoclinic and orthorhombic $NbOPO_4$ is clearly first order, whereas the displacive tetragonal-to-tetragonal $NbOPO_4$ phase transition is apparently second order. Furthermore, the negative thermal expansion behavior for orthorhombic $NbOPO_4$ is much more pronounced than that for high-temperature tetragonal $NbOPO_4$. For tetragonal $NbOPO_4$ at high temperatures, only one cell edge shows negative thermal expansion, and the average linear thermal expansion is $+6\times10^{-6}/°C$. For orthorhombic $NbOPO_4$, all cell edges show negative thermal expansion above 400°C, and the average linear thermal expansion is $-3.7\times10^{-6}/°C$. This very big difference in negative thermal expansion behavior is likely largely attributable to the relative openness of the two structures. At room temperature tetragonal $NbOPO_4$ is 18% denser than monoclinic $NbOPO_4$. A similar situation exists for SiO_2, where the usual dense forms such as quartz show little or no negative thermal expansion behavior, but in the open faujasite structure there is strong negative thermal expan-

TABLE 6
Selected Bond Distances for 325 and 400°C Data

[2] Nb–O(1)	Nb–O(2)	[2] Nb–O(3)	Nb–O(4)
1.882(2)[a]	1.934(6)	2.020(4)	1.968(6)
1.881(2)	**1.950(4)**	**2.012(3)**	**1.958(4)**
P–O(2)	[2] P–O(3)	P–O(4)	
1.539(6)	1.490(4)	1.526(6)	
1.529(5)	**1.497(3)**	**1.531(4)**	

[a]Bold values are for 400°C; others are for 325°C.

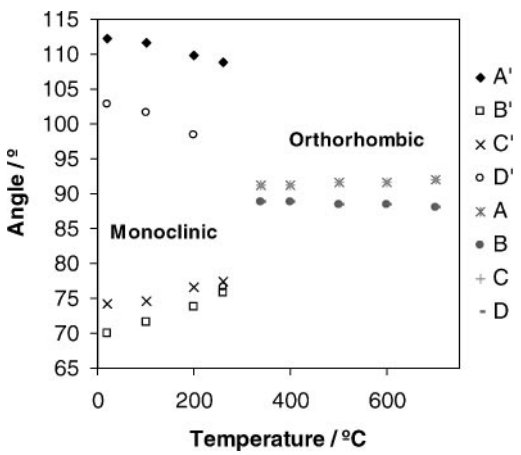

FIG. 9. Tilt angles vs temperature.

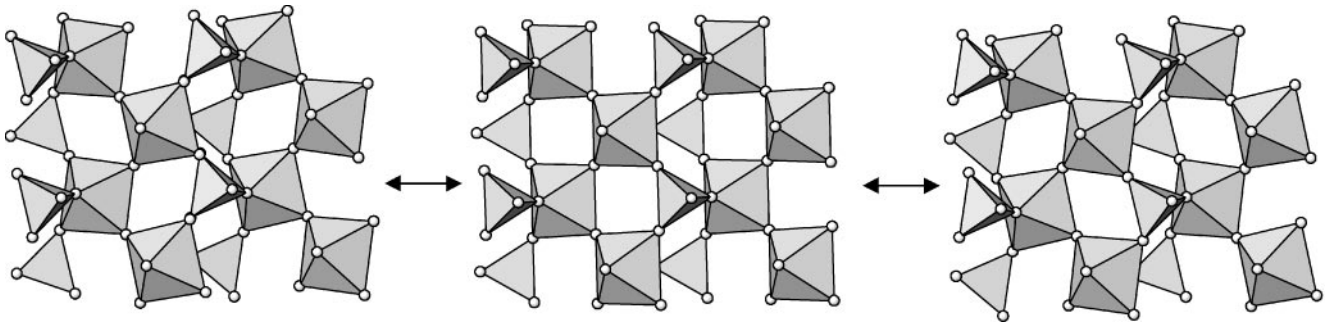

FIG. 10. The *bc* plane of the $NbOPO_4$ structure showing the rocking motion which gives the negative thermal expansion of *b* and *c* at high temperatures.

sion over a broad temperature range (7). The assumption is that the large transverse thermal motions of oxygen atoms can interfere with each other in the denser structures.

The Nb–O–Nb and Nb–O–P angles labeled ABCD in Fig. 1 are plotted vs temperature in Fig. 9. These angles are close to 90° in orthorhombic $NbOPO_4$ but deviate strongly from 90° in monoclinic $NbOPO_4$. This plot nicely shows the first-order nature of this monoclinic-to-orthorhombic phase transition. The displacements of atoms on going from monoclinic $NbOPO_4$ at 25°C to orthorhombic $NbOPO_4$ at 325°C are tabulated in Table 8. The largest displacements are related to O(1) and O(3) of orthorhombic $NbOPO_4$ (Fig. 6). The large and highly anisotropic thermal motion of these oxygen atoms is evident in Fig. 6 and Table 7. On cooling through the phase transition, these large thermal motions are frozen to give the displacements shown in Table 8. The correlated nature of the transverse thermal motions of oxygen is treated as rocking motions of the polyhedra (Fig. 10). The structure in the center is that of orthorhombic $NbOPO_4$; those on either side are monoclinic $NbOPO_4$, tilted in opposite directions. Above 292°C the polyhedra rock back and forth as shown in Fig. 10, and this gives the negative thermal expansion in the *bc* plane. Below 292°C the thermally activated rocking motions have decreased to the point where the structure is trapped in the tilted form, and now the thermal expansion in the *bc* plane is positive.

Distance least-squares (DLS) calculations (8) indicate that the monoclinic $NbOPO_4$ structure can be built of perfectly regular polyhedra. However, the orthorhombic $NbOPO_4$ with fewer free parameters cannot be built from perfectly regular polyhedra. In the monoclinic structure, setting all Nb–O distances equal to 1.99 Å and all P–O distances to 1.52 Å, the cell dimensions refine to

TABLE 7
Refined Anisotropic Thermal Parameters (Å^2) for 325 and 400°C Data

Atom	100**U*11	100**U*22	100**U*33
Nb	0.7(1)[a]	1.5(1)	1.5(1)
	0.97(9)	**1.5(1)**	**1.4(1)**
P	1.6(2)	1.2(2)	0.6(2)
	1.6(1)	**1.2(1)**	**1.2(1)**
O(1)	2.3(2)	5.3(3)	0.7(2)
	2.8(2)	**5.1(2)**	**0.8(1)**
O(2)	1.1(2)	3.8(3)	3.4(3)
	1.0(2)	**4.0(2)**	**3.8(2)**
O(3)	4.0(2)	0.8(1)	7.3(3)
	4.5(1)	**1.1(1)**	**7.1(2)**
O(4)	1.4(2)	3.0(2)	3.7(3)
	1.5(1)	**3.4(2)**	**3.4(2)**

[a]Bold values are for 400°C; others are for 325°C.

TABLE 8
Distance between Monoclinic and Equivalent Orthorhombic Atoms

Monoclinic atom (25°C)	Orthorhombic atom (325°C)	*d*/Å
Nb(1)		0.035
	Nb	
Nb(2)		0.041
P(1)		0.077
	P	
P(2)		0.107
O(3)		0.303
	O(1)	
O(8)		0.247
O(2)		0.089
	O(2)	
O(7)		0.191
O(4)		0.342
O(5)		0.231
	O(3)	
O(9)		0.222
O(10)		0.340
O(1)		0.045
	O(4)	
O(8)		0.099

$a = 11.23$ Å, $b = 5.39$ Å, $c = 6.62$ Å, and $\beta = 92.2°$. However, when the same distances are used in the orthorhombic structure, the residual increases and the cell dimensions obtained are $a = 11.31$ Å, $b = 5.32$ Å, and $c = 6.66$ Å. The distortion of the polyhedra can be related to the A–C and B–D lengths in Fig. 1. The tetrahedron edge is smaller than the octahedron edge, making the A–C and B–D lengths unequal. If the distances are adjusted in the DLS program so that the A–C, A–B, C–D, and B–D lengths are all equal, the residual is reduced but the O–P–O angle associated with A–C has increased to 117° and the cell edges have become $a = 11.37$ Å, $b = 5.42$ Å, and $c = 6.49$ Å.

Attempts to quench the orthorhombic form of $NbOPO_4$ to room temperature by rapid cooling through the 292°C phase transition were unsuccessful. In principle, quenching the high-temperature form is possible because DSC indicates that the phase transition is first order. However, the phase transition is displacive rather than reconstructive. Thus, an activation barrier high enough to allow quenching of the high-temperature form seems unlikely, consistent with our results. Nonetheless, orthorhombic $NbOPO_4$ has been reported at room temperature (3). Possible explanations are that orthorhombic $NbOPO_4$ was stabilized at room temperature by impurities or nonstoichiometry.

ACKNOWLEDGMENTS

This research was supported by NSF Grant DMR 9802488. We acknowledge the support of the National Institute of Standards and Technology, U.S. Department of Commerce, in providing the neutron research facilities used in this work.

REFERENCES

1. J. M. Longo and P. Kierkegaard, *Acta Chem. Scand.* **20,** 72 (1966).
2. A. LeClaire, H. Chahboun, D. Groult, and B. Raveau, *Z. Kristallogr.* **177,** 277 (1986).
3. D. L. Serra and S.-J. Hwu, *Acta Crystallogr. C* **48,** 733 (1992).
4. T. G. Amos, A. Yokochi, and A. W. Sleight, *J. Solid State Chem.* **14,** 303 (1998).
5. A. C. Larson and R. B. von Dreele, "LANSCE." Los Alamos National Laboratory, Los Alamos, NM, 1994; W. A. Dollase, *J. Appl. Crystallogr.* **19,** 267 (1986).
6. P. M. Forster and A. W. Sleight, *Int. J. Inorg. Mater.* **1,** 123 (1999).
7. M. P. Attfield and A. W. Sleight, *Chem. Commun.* 601 (1998).
8. W. M. Meier and H. Villiger, *Z. Kristallogr.* **129,** 161 (1996).